Indian Journal of Biochemistry & Biophysics
Vol. 59, August 2022, pp. 823-835
DOI: 10.56042/ijbb.v59i8.55954

Design and synthesis of novel quercetin metal complexes as IL-6 inhibitors for anti-inflammatory effect in SARS-CoV-2

Akey Krishna Swaroop[1], Sunil Kumar Patnaik[1], Vasanth P[2], Jeyaprakash MR[3], Praharsh Kumar MR[4] & Jawahar N[4] & Jubie S[1]*

[1]Department of Pharmaceutical Chemistry; [2]Department of Biotechnology; [3]Department of Pharmaceutical Analysis; & [4]Department of Pharmaceutics, JSS College of Pharmacy, JSS Academy of Higher Education & Research Ooty-643 001, Tamil Nadu, India

Received 07 October 2021; *revised 18 May 2022*

One of the most common causes of mortality in COVID-19 patients is cytokine release syndrome (CRS). Though several cytokines are involved in CRS, the role of Interleukin 6 is significant. Considering the importance of IL-6 inhibition and the drawbacks of the existing monoclonal antibodies, the present study develops new flavonoid metal complexes as immune boosters targeting IL-6 for SARS-CoV-2 treatment. To identify the potential flavonoids from 152 secondary plant metabolites, PyRx 0.9 tool has been used. The top scorer quercetin was converted into quercetin-oxime. Seven metal complexes (QM-1 to QM-7) were made from quercetin-oxime by utilizing divalent metals such as zinc, copper, magnesium, cobalt, barium, and cadmium. It was assumed that all compounds were moderately soluble and would not penetrate the BBB through *in silico* ADME studies. However, the *in vitro* heamolytic research revealed a modest heamolytic effect in all seven complexes. To know the IL-6 inhibitory potential preliminary level, the complexes were screened for cytotoxicity in cell lines MCF-7 which predominantly expresses the IL-6 level. The cytotoxic effects of all complexes were considerable relative to the marketable Nutridac formulation. The complexes quercetin-Zinc (QM1) and quercetin-Zinc-Ascorbic acid (QM7) showed significant cytotoxicity on MCF-7 compared to Nutridac and no cytotoxic toward the normal cell lines.

Keywords: Anti-inflammatory, Cytokine release syndrome, Haemolytic, Nutridac

The new data shows that the Coronavirus has been a fresh epidemic worldwide for one and half years. In December 2019, it was initially identified in Wuhan, China. The Coronavirus is a massive family strain of the family of coronaviridae[1]. Firstly, this virus was transferred to people through infected animals (bats and pangolins) and then spread worldwide[2]. Recent studies indicate that many individuals infected with COVID-19 may die due to their excessive response to immune systems, which leads to the abnormal production of cytokines known as cytokine release syndrome (CRS)[3,4]. CRS affects the decline and deterioration of COVID-19 pneumonic patients who develop acute respiratory stress syndrome (ARDS)[5,6]. CRS is a systemic inflammatory response characterized by a significant increase of pro-inflammatory cell cytokines in response to infection, certain medicines, or other reasons[7-9]. It is a term that denotes an overactive immune response that is characterized by the production of interferons, interleukins, tumour necrosis factor-alpha (TNF-α), chemokines, and other proteins[4,6,10,11].CRS is a frequent immunopathogenesis that may result in acute respiratory distress syndrome (ARDS), sepsis, graft-*vs*-host disease (GvHD), rheumatoid arthritis-induced macrophage activation syndrome (MAS), and primary and secondary hemophagocytic lymphohistiocytosis (HLH)[12]. Numerous cytokines, including IL-6, IL-1, IL-2, IL-10, TNF-α, and IFN-γ, are implicated in the 'cytokine storm' in many COVID-19 patients; however, IL-6 seems to play a significant role, with increased levels associated with dyspnea, ARDS, and poor clinical outcomes[13,14]. While the IL-6 cytokine plays a substantial role as an inflammatory mediator in innate and adaptive immune responses, it may also have anti-inflammatory and protective properties in some clinical circumstances[15]. New research on COVID-19 patients indicates that IL-6 and its receptors may have significant diagnostic and therapeutic potential.

A potent pro-inflammatory agent, IL-6 works through two major signaling pathways: cis and trans. Cis-signaling involves IL-6 joining the membrane-bound IL-6 receptor and Gp130 to activate Janus kinases (JAKs) and signal transducer and activator of

*Correspondence:
E-mail: jubie@jssuni.edu.in

transcription 3 (STAT3)[1]. These pleiotropic effects on the acquired immune system (B and T cells) and the innate immune system (neutrophils, macrophages, and natural killer cells) may lead to CRS when activated. To activate trans-signaling, significant levels of IL-6 in the blood bind to the solubilized version of the receptor (sIL-6R) in most somatic cell types[16]. To stimulate IL-6–sIL-6R–JAK-STAT3 signaling in cells lacking mIL-6R, such as endothelial cells, increases the "cytokine storm" by secreting VEGF, MCP-1, IL-8, and IL-6 while decreasing E-cadherin expression on endothelial cells. VEGF secretion and reduced E-cadherin expression led to vascular permeability and leakage, contributing to hypotension and pulmonary dysfunction in ARDS[17-19].

IL-6 and IL-6R antagonists have previously shown effectiveness in treating CRS and secondary hemophagocytic lymphohistiocytosis (sHLH), both of which cause blood cytokine elevation. This CRS implicates IL-6 in the pathogenesis of cytokine-driven hyperinflammatory disorders and makes it a possible COVID-19 target[5]. The increasing scientific evidence for flavonoids' potential to relieve inflammatory diseases and their safe and cost-effective characteristics has led to the development of new flavonoid-inspired nutraceuticals and therapies. The deficit of metals impacts plasma cytokines such as TNF-α and, IL-1, IL-6, whereas metal supplementation has a dose-dependent effect[19,20,29]. The goal is to design and produce novel flavonoid metal complexes as immune boosters for treatment with SARS-CoV-2. We report the synthesis, characterization, and cytotoxicity investigations of flavonoid metal complexes to build new "leads" which act as Interleukin-6 antagonists.

Materials and Methods

Solvents and reagents of analytical and laboratorygrade were used in the synthesis process. Chemicals were dried and cleaned by established procedures. TLC analysis was used to monitor the reactions and determine the purity of the products. We utilized 60-F 254 (0.5 mM) MERCK aluminum back pre-coated silica gel plates for thin-layer analytical chromatography. Carousel Radleys Parallel organic synthesizer was used for the final synthesis. The absorbance of substances was determined using a Shimadzu UV-visible spectrometer. The FT-IR spectrometer from Perkin-Elmer was used to determine the IR spectra. The ^{1}H- and ^{13}C-NMR spectra were obtained using a BRUKER (400MHz FT-NMR) in DMSO solvent with TMS serving as an internal standard. Shimadzu LC-MS was used to determine the mass spectra of the compounds. Carbanio.com supplied quercetin (2- (3, 4 dihydroxyphenyl)-3, 5, 7-trihydroxy-4H-chromene-4-one). All chemical products used in reagent preparation were weighed with an accuracy of 0.0001 g. Solvents were cleaned and dried in line with industry requirements.

Molecular docking

PyRx 0.8 was used to perform the docking research. PyRx is a Python-based programming language that runs on almost any contemporary machine, from personal computers to supercomputers. PyRx has been used to determine the binding affinity of a ligand to a protein to facilitate molecular docking.The workflow of our study is depicted in (Fig. 1). PyRx, a structure-based docking program, was used to screen all 152 secondary metabolites for IL-6 (PDB: 1ALU) at a resolution of 1.90. Additionally, ligands for energy reduction interact in good ways. The MMFF94 force field performed the minimization in 200 steps with an RMS gradient of 0.1. Following the devaluation, the ligands were transferred to PDBQT format. First, we had chosen the macromolecule that will define the produced protein's binding site. Next, the active docking site was constructed utilizing bound ligand binding locations. Then, virtual screening was performed on a molecular window, with all produced ligands interacting with the specified active site[21,22]. Next, all ligands according to their binding affinity as determined by the PyRx score. Following that, the ligands were classified according to their binding energy levels. The top

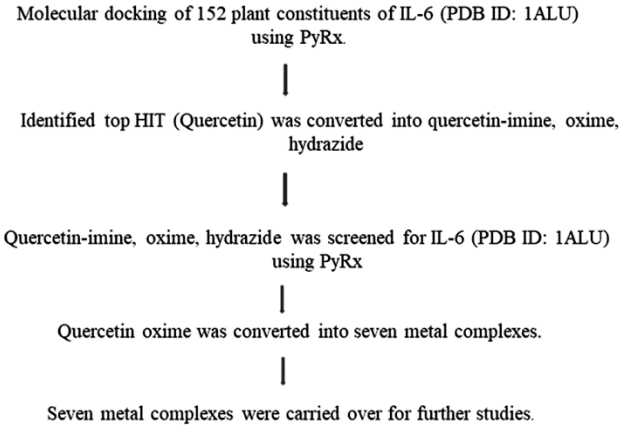

Fig. 1 —Workflow of our study

scorer quercetin was converted into imines, oximes, and hydrazides. The docking analysis for these analogs was then re-evaluated and re-constructed by the binding energy estimations.

ADME and toxicity prediction

ADME properties were estimated using the SwissADME tool, and toxicity properties were calculated using the online bioinformatics tool PreADMET. ADMET studies were conducted for designed metal complexes, such as their aqueous solubility, blood-brain barrier (BBB), plasma protein binding (PPB), hepatotoxicity, polar surface area, cytochrome P450, CYP2D6 inhibition, human gut absorbance, rodent carcinogenicity, Ames mutagenicity and toxicology potential development. A logP value that indicates lipophilicity in a molecule is the partition coefficient value in an octanol/water system. LogP is an important metric that reflects the impact on bioavailability, distribution, volume clearance, and membrane permeability. Diverse tissues have been investigated in this study with the expectations and significant characteristics of the compounds, such as mutagenicity and toxicity. The PreADMET serve has predicted pharmacologically relevant properties[30].

Synthesis of Quercetin oxime (QO)

A combination of hydroxylamine hydrochloride (0.01 mol, 0.69 g), quercetin (0.01 mol, 5.8 g), and sodium acetate trihydrate (0.01 mol, 1.36 g) diluted in 25 mL ethanol (0.01 mol) were heated at reflux on a water bath with continuous mixing for 4 h. A yellow solid precipitated out during ambient temperature (80°C) was filtered, cleaned, and dried under a vacuum[23].

General procedure for the synthesis of quercetin oxime metal complexes (QM1-QM6)

The proposed metal complexes were synthesized using the metal salts $Zncl_2$, $CuCl_2$, $CoCl_2$, $MgCl_2$, $BaCl_2$, and $CdCl_2$ in a 1:2 stoichiometric ratio. First, the quercetin oxime binder was dissolved in a metal salt solution in 10 mL of ethanol and 10mL distilled water. Following this time, the complete precipitation of the produced compounds was kept at low temperatures (cooler) for two days before being filtered into a porous drying platform and sucked in a desiccator[24].

General procedure for the synthesis of quercetin ascorbic acid metal complex (QM7)

One analog was developed as a bi-ligand containing quercetin, zinc, and ascorbic acid in a 1:1:1 ratio. The complex was produced in a stoichiometric ratio of 1:1:1 using metal salt Zncl2 with quercetin and ascorbic acid as ligands. The quercetin and ascorbic acid binder were mixed with 10 mL ethanol. The metal salt was dissolved in 10 mL of distilled water. The mixture was stirred continuously for 3 h at room temperature (27°C). The solution was cooled ata lower temperature (cooler) for two days before being filtered through a porous plate funnel and vacuum-sealed in a desiccator.

(4Z)-2- (3, 4-dihydroxyphenyl)-4- (hydroxyimino)-4H-chromene-3, 5, 7-triol (QO)

Yellow crystal; Rf value= 0.78 (Toluene: Ethyl acetate: Formic acid. 5:4:0.2., *v/v* developer, visualization: UV and I_2), yield 91%. M.p 295-300°C. M.F: $C_{15}H_{11}NO_7$; MW: 317. UV-Visible (nm): 203, 256, 305, 374 (bands formed), FTIR (KBr, cm^{-1}): 3264.63 (O-H str), 1614.47 (C=N str), 1141.90 (C-OH str), 1169.87 (C-O-C str), 789.98 (C-H strAr), 1558.54 (C=C str). ^{1}H NMR (300 MHZ, DMSO) δ 10.04 (s, IH, OH_1), 11.02 (s, 1H, OH_2), 9.4 (s, IH, OH_5), 8.6 (s, 1H, OH_6), 7.9 (m, 5H, Ar-H_1), 7.7 (m, 5H, Ar-H_2), 12.72 (s, IH, $^OH_3$), 10.57 (s, IH, OH4) MS: 317.05 (M^+).

5, 5′-bis (3, 4-dihydroxyphenyl)-8, 8′, 10, 10′-tetrahydroxy-3, 3′-spirobi[chromeno[4, 3-e]1, 3-dioxa-4-aza-2-zincacyclohexane]-3, 3-diuide (QM1)

Greenish black; Rf value= 0.52 (Toluene: Ethyl acetate: Formic acid. 5:4:0.2., *v/v* developer, visualization: UV and I_2), yield 85%. M.p >300°C. M.F: $ZnC_{30}H_{18}N_2O_{14}$; MW: 694.006. UV-Visible (nm): 257, 298, 302, 375 (bands formed), FTIR (KBr, cm^{-1}): 3382.29 (O-H str), 1645.33 (C=N str), 1274.03 (C-OH str), 1086.92 (C-O-C str), 2975.30 (C-H str Ali), 1543.10 (C=C str), 879.57 (C-H strAr), 668.38, 1047.38, 1391.69 (Zn-O). ^{1}H NMR (300 MHZ, DMSO)δ 10.04 (s, IH, OH_1), 9.8 (s, 1H, OH_2), 9.4 (s, IH, OH_5), 8.6 (s, 1H, OH_6), 7.9 (m, 5H, Ar-H_1), 7.7 (m, 5H, Ar-H_2), 7.5 (s, IH, OH_3), 7.14 (s, IH, OH4), 7.06 (s, IH, OH_7), 6.9 (s, IH, OH_8), MS:694.006 (M^+).

5, 5′-bis (3, 4-dihydroxyphenyl)-3, 3′-spirobi[chromeno[4, 3-e]1, 3-dioxa-4-aza-2-cupracyclohexane]-8, 8′, 10, 10′-tetrol (QM2)

Black powder; Rf value= 0.36 (Toluene: Ethyl acetate: Formic acid. 5:4:0.2., *v/v* developer, visualization: UV and I_2), yield 79%. M.p >300°C. M.F: $CuC_{30}H_{18}N_2O_{14}$; MW: 693.001. UV-Visible(nm): 257, 297 (bands formed), FTIR (KBr, cm^{-1}): 3456.55 (O-H str), 1619.29 (C=N str), 1295.24 (C-OH str), 1114.89 (C-O-C str), 771.54 (C-H strAr), 1558.54 (C=C str), 668.36, 1345.39 (Cu-O), ^{1}H NMR

(300 MHZ, DMSO)δ 10.07 (s, IH, OH_1), 9.8 (s, 1H, OH_2), 9.5 (s, IH, OH_5), 8.65 (s, 1H, OH_6), 7.8 (m, 5H, Ar-H_1), 7.7 (m, 5H, Ar-H_2), 7.5 (s, IH, OH_3), 7.14 (s, IH, OH4), 7.06 (s, IH, OH_7), 6.8 (s, IH, OH_8) MS: 694.01 (M^+).

5, 5′-bis (3, 4-dihydroxyphenyl)-3, 3′-spirobi[chromeno[4, 3-e]1, 3-dioxa-4-aza-2-magnesacyclohexane]-8, 8′, 10, 10′-tetrol (QM 3)

Yellow powder; Rf value= 0.21 (Toluene: Ethyl acetate: Formic acid. 5:4:0.2., *v/v* developer, visualization: UV and I_2), yield 86%. M.p >300°C. M.F: $MgC_{30}H_{18}N_2O_{14}$; MW: 654.060. UV-Visible (nm): 203, 256, 302, 374 (bands formed), FTIR (KBr, cm^{-1}): 3461.38 (O-H str), 1654.01 (C=N str), 1263.42 (C-OH str), 1169.87 (C-O-C str), 721.40 (C-H strAr), 1559.90 (C=C str), 459.07, 611.45, 1092.71 (Mg-O), ^{1}H NMR (300 MHZ, DMSO)δ 10.06 (s, IH, OH_1), 9.9 (s, 1H, OH_2), 9.5 (s, IH, OH_5), 8.65 (s, 1H, OH_6), 7.8 (m, 5H, Ar-H_1), 7.68 (m, 5H, Ar-H_2), 7.5 (s, IH, OH_3), 7.20 (s, IH, OH4), 7.06 (s, IH, OH_7), 6.8 (s, IH, OH_8) MS: 654.060 (M^+).

5, 5′-bis (3, 4-dihydroxyphenyl)-3, 3′-spirobi[chromeno[4, 3-e]1, 3-dioxa-4-aza-2-cobaltacyclohexane]-8, 8′, 10, 10′-tetrol (QM4)

Yellow powder; Rf value= 0.42 (Toluene: Ethyl acetate: Formic acid. 5:4:0.2., *v/v* developer, visualization: UV and I_2), yield 86%. M.p >300°C. M.F: $BaC_{30}H_{18}N_2O_{14}$; MW: 767.981. UV-Visible (nm): 256, 302, 374 (bands formed), FTIR (KBr, cm^{-1}): 3439.19 (O-H str), 1623.15 (C=N str), 1265.35 (C-OH str), 1169.87 (C-O-C str), 725.26 (C-H strAr), 1557.57 (C=C str), 570.95, 639.42, 1028.09 (Co-O), ^{1}H NMR (300 MHZ, DMSO)δ 10.05 (s, IH, OH_1), 9.76 (s, 1H, OH_2), 9.39 (s, IH, OH_5), 8.65 (s, 1H, OH_6), 7.8 (m, 5H, Ar-H_1), 7.6 (m, 5H, Ar-H_2), 7.5 (s, IH, OH_3), 7.14 (s, IH, OH4), 7.06 (s, IH, OH_7), 6.9 (s, IH, OH_8) MS: 689.403 (M^+).

5, 5′-bis (3, 4-dihydroxyphenyl)-3, 3′-spirobi[chromeno[4, 3-e]1, 3-dioxa-4-aza-2-baracyclohexane]-8, 8′, 10, 10′-tetrol (QM5)

Brown powder; Rf value= 0.64 (Toluene: Ethyl acetate: Formic acid. 5:4:0.2., *v/v* developer, visualization: UV and I_2), yield 86%. M.p >300°C. M.F: $CoC_{30}H_{18}N_2O_{14}$; MW: 689.008. UV-Visible (nm): 256, 304, 373 (bands formed), FTIR (KBr, cm^{-1}): 3473.91 (O-H str), 1703.20 (C=N str), 1320.32 (C-OH str), 1169.87 (C-O-C stretching), 717.54 (C-H strAr), 1618.33 (C=C stretch), 459.07, 644.25, 1002.05 (Ba-O), ^{1}H NMR (300 MHZ, DMSO) δ 10.04 (s, IH, OH_1), 9.8 (s, 1H, OH_2), 9.4 (s, IH, OH_5), 8.6 (s, 1H, OH_6), 7.9 (m, 5H, Ar-H_1), 7.7 (m, 5H, Ar-H_2), 7.5 (s, IH, OH_3), 7.14 (s, IH, OH4), 7.06 (s, IH, OH_7), 6.9 (s, IH, OH_8)MS: 767.797 (M^+).

5, 5′-bis (3, 4-dihydroxyphenyl)-3, 3′-spirobi[chromeno[4, 3-e]1, 3-dioxa-4-aza-2-cadmacyclohexane]-8, 8′, 10, 10′-tetrol (QM6)

Yellow powder; Rf value= 0.40 (Toluene: Ethyl acetate: Formic acid. 5:4:0.2., *v/v* developer, visualization: UV and I_2), yield 86%. M.p >300°C. M.F: $CdC_{30}H_{18}N_2O_{14}$; MW: 743.979. UV-Visible (nm): 202, 257, 373 (bands formed), FTIR (KBr, cm^{-1}): 3277.17 (O-H str), 1653.05 (C=N str), 1237.78 (C-OH str), 1173.72 (C-O-C str), 745.51 (C-H strAr), 1623.15 (C=C str), 506.33, 556.48, 1003.02 (Ba-O), ^{1}H NMR (300 MHZ, DMSO)δ 10.07 (s, IH, OH_1), 9.88 (s, 1H, OH_2), 9.3 (s, IH, OH_5), 8.6 (s, 1H, OH_6), 7.9 (m, 5H, Ar-H_1), 7.7 (m, 5H, Ar-H_2), 7.5 (s, IH, OH_3), 7.18 (s, IH, OH4), 7.1 (s, IH, OH_7), 6.9 (s, IH, OH_8)MS: 742.881 (M^+).

6′- (1, 2-dihydroxyethyl)-4- (3, 4-dihydroxyphenyl)-7, 9-dihydroxy-4′-oxo-4′, 6′-dihydro-9bH-spiro[1, 3-dioxa-2zincacyclopenta[4, 5-c]chromene-2, 2′-furo[3, 4-d]1, 3-dioxa-2-zincacyclopentane]-2, 2-diuide (QM7)

Yellow powder; Rf value= 0.27 (Toluene: Ethyl acetate: Formic acid. 5:4:0.2., *v/v* developer, visualization: UV and I_2), yield 84%. M.p >300°C. M.F: $ZnC_{21}H_{16}O_{13}$; MW: 552.983. UV-Visible (nm): 224, 227, 236, 279 (bands formed), FTIR (KBr, cm^{-1}): 3442.09 (O-H str), 1704.17 (C=O str), 1249.91 (C-OH str), 1168.90 (C-O-C str), 2847.99 (C-H str Ali), 647.09 (C-H strAr), 1575.89 (C=C str), 479.33, 515.01, 1020.38 (Zn-O), ^{1}H NMR (300 MHZ, DMSO)δ 10.04 (s, IH, OH_1), 9.8 (s, 1H, OH_2), 9.4 (s, IH, OH_5), 8.6 (s, 1H, OH_6), 7.9 (m, 5H, Ar-H_1), 7.7 (m, 5H, Ar-H_2), 4.86 (s, IH, OH_3), 3.45 (s, IH, OH4), 5.80 (d, IH, Ar-H_3), 3.43 (s, IH, Al-H_1), 3.45 (s, IH, Al-H_2), 3.73 (s, IH, Al-H_3) MS: 541.754 (M^+).

Biological studies

Haemolytic assay

A fresh blood sample from a retro-orbital rat was collected, spun for 10 min at 2000 rpm, and used to determine the heamolytic activity of produced compounds. The 0.9 percent NaCl solution was resuspended in the cell pellet to produce a 2 percent (*v/v*) cell suspension. A 100 µL suspension of red blood cells was added to the whole 96-well plate and incubated for 1 hour at 37°C with 5% CO2. The release of Haemoglobin was determined by spectrometric supernatant analysis at 540 nm as an indicator of red blood cell breakdown (RBC) (haemolysis). Complete haemolysis was obtained (positive control) by adding

1% (*v/v*) NaOH, while cells were negative in 0.9 percent (*w/v*) NaCl solution[25].

Cell lines and culture medium

MCF-7 cell cultures were obtained from India's National Centre for Cell Sciences in Pune. The cells were cultured in Dulbecco's modified Eagle's medium (DMEM) supplemented with Fetal Calf Serum, trypsin (0.5 g/L), EDTA (197.16 mg/L), and PBS (1 L) and maintained at 37°C in a CO_2 incubator. This solution was used to subculture adherent cells. After removing the medium, ten milliliters of trypsin/EDTA were added to this combination and incubated. Next, 10 mL DMEM medium was added and transferred to the centrifuge tube in the flask. For 5-7 min, the cells were spun at 1300-1500 rpm[26].

MTT assay

DMEM media with 10% FBS was used to trypsinize the monolayer cell culture and adjust the cell count to 1 × 10^4 cells/well. 100 µL of the diluted cell suspension (about 10, 000 cells/well) was put to each well of a 96-well microtiter plate. The supernatant was discarded after 24 h when a partial monolayer had developed. The monolayer was washed with medium once. Different concentrations of test samples (100 µL) were applied to the partial monolayer in each well of microtiter plates. After that, the plates were incubated at 37°C for 72 h in a 5% CO_2 environment. Every 24 h, microscopic inspections and observations were made. After 72 h, the sample solutions in the wells were removed, and each well was filled with 20 µL of MTT (2 mg/mL) in MEM-PR (MEM without phenol red). The plates were gently shaken and incubated at 37°C in a 5% CO2 environment for 3 h. The supernatant was removed, and 50 µL of isopropanol was added, followed by gently shaking the plates to dissolve the formazan produced. The absorbance was determined at a wavelength of 540 nm using a microplate reader. The percentage inhibition of cell growth was computed using the following formula, and the concentration of the medication or test sample required to inhibit cell growth by 50% was determined using the dose-response curves for each cell line[26-28].

Results and Discussion

In silico design

The 3D structure of the human protein interleukin-6 was collected from the protein data bank (PDB: 1ALU). The active site amino acid residues were identified from the protein-ligand interaction profile (PLIP). The amino acid residues present in a catalytic pocket are *Gln183, Phe78, Gln75, Ser76, Ala180, Arg179, Cys78, Glu69, Ser176, Met67, Gln175, Phe173, Lys171, Lys66, Pro65, Ser169, and Glu172* shown in (Fig. 2).The prepared protein was validated by the Ramachandran plot (Fig. 3).

In PyRx, binding affinity parameters were considered for selecting the best "HITS" and compared with the known inhibitor Curcumin. PyRx binding energy is the interaction energy between the protein and the ligand. This value strongly indicates the extent of the interaction of proteins and ligands. Quercetin (−6.9 kcal/mol) showed the highest binding affinity among all the 152 selected plant secondary metabolites whose binding energy was above standard Curcumin (−5.8 kcal/mol) and co-crystal (tartaric acid) (−4.7 kcal/mol). Among the analogs designed, quercetin oxime (−7.0 kcal/mol) showed the highest binding affinity. The binding energy of the top ten compounds and analogous, as shown in (Table 1) and (Table 2).

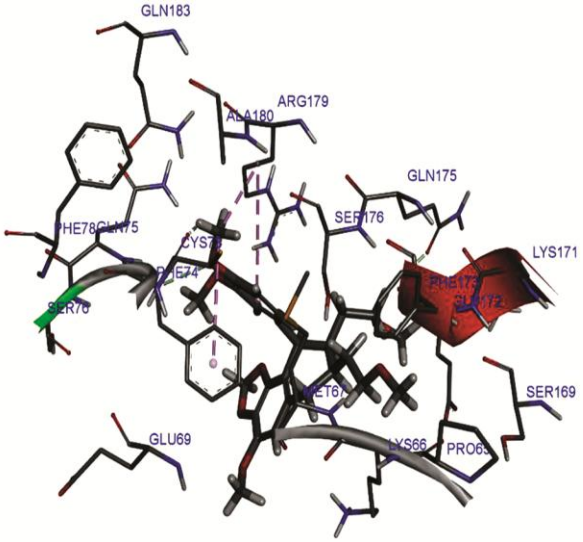

Fig. 2 —Amino acids present in the active site of the catalytic pocket of the IL-6 receptor (PDB id: 1ALU)

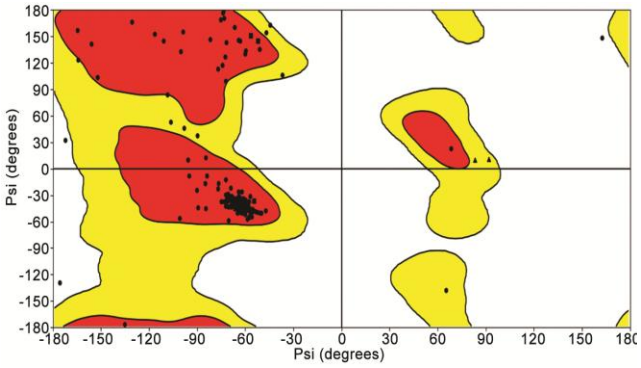

Fig. 3 — Ramachandran plot of 1ALU

Table 1 — List of plant secondary metabolites and Binding energies

S. No:	Compound	Chemical Structure	Binding affinity
1	Quercetin	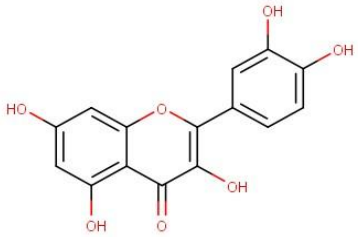	−6.9
2	Myricetin	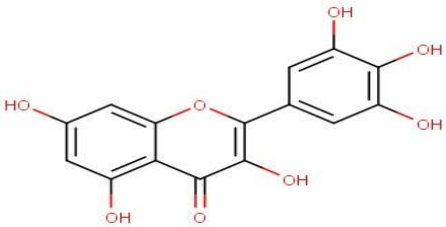	−6.5
3	Epigallocatechin	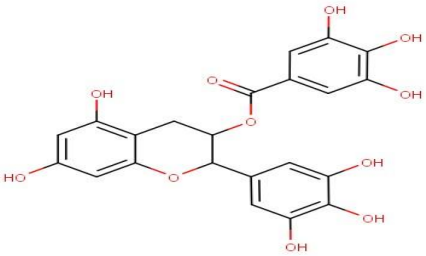	−6.5
4	Eupalitin	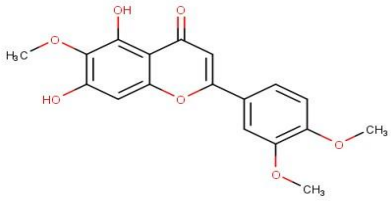	−6.4
5	Laurifolin	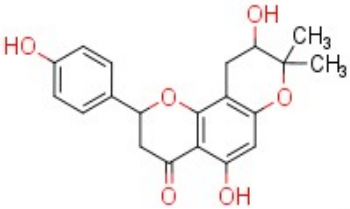	−6.4
6	Naringenin		−6.2
7	Aromadendrin	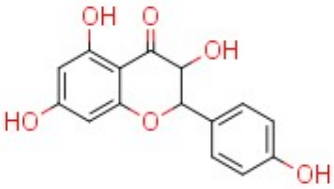	−6.0

(*Contd.*)

Table 1 — List of plant secondary metabolites and Binding energies (*Contd.*)

S. No:	Compound	Chemical Structure	Binding affinity
8	Arjunone	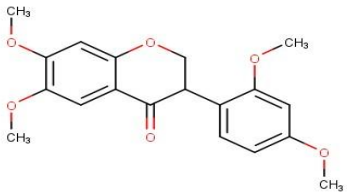	−6.0
9	Andrographolide	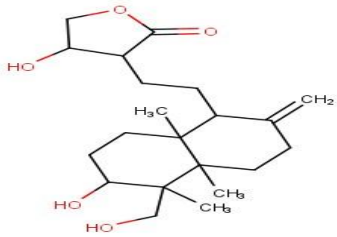	−5.9
10	Boeravinone G	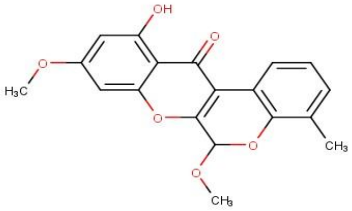	−5.8
11	Curcumin	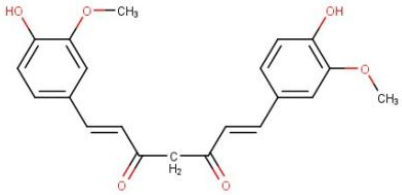	−5.8
12	Tartaric acid (co-crystal)	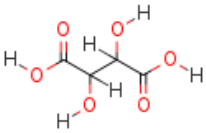	−4.7

Table 2 — List of designed scaffolds and Binding energies.

S. No:	Compound	Chemical Structure	Binding affinity
1	Quercetin hydrazide	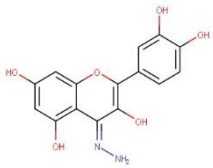	−6.7
2	Quercetin imine	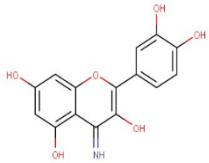	−6.5
3	Quercetin oxime		−5.6

2D interactions of quercetin IL-6 complex, quercetin oxime IL-6 complex and tartaric acid IL-6 complex were shown in (Fig. 4A-C). Synthesized metal complexes are shown in (Table 3).ADME properties of designed compounds (SwissADME) are shown in (Table 4). Toxicity studies for designed compounds (http://preadmet.bmdrc.org/) are shown in (Table 5).

Chemistry

We synthesized quercetin oxime from quercetin through the Beckmann rearrangement process, which converts the ketone to the ketoxime. The reaction is unusual in that no byproduct is produced. Metal complexes of quercetin oxime were produced from quercetin oxime in a 1:2 ratio using metal chlorides [$ZnCl_2$, $CuCl_2$, $COCl_2$, $MgCl_2$, $BaCl_2$, $CdCl_2$].

Quercetin oxime was able to form complexes with various cations due to the presence of chelating sites in its structure. Chelating characteristics of quercetin oxime are dictated by their chemical structure, which consists of two aromatic rings, benzoyl ring A and cinnamoyl ring B, connected by anO-heterocycle. The 3-hydroxychromone, 4-N-hydroxychromone, and 3′, 4′-dihydroxyl groups are potentially chelating sites for (Scheme 1). They were made from quercetin and ascorbic acid using metal chlorides [ZnCl2] in a 1:1:1 ratio. Quercetin and ascorbic acid may form complexes with various cations due to chelating sites in their structure. The molecular structure of quercetin determines its chelating properties: two aromatic rings (benzoyl ring A and cinnamoyl ring B) linked by an O-heterocycle. The 3′, 4′-dihydroxyl, and 5-hydroxychromone groups are potential chelating sites. The chelating effects of ascorbic acid are governed by its ring structure, with different hydroxy groups linked by O-heterocycle for (Scheme 1).

Biological studies

Haemolytic assay

For hemolytic activity, the metal complexes were tested at various concentrations (25, 50, and 100 µg/mL). 50 µg/mL showed little haemolysis. The explicit or implicit impact of chemicals on blood cells necessitates nanotoxicology research. The movement of erythrocytes through many organs damages DNA and membranes and causes congenital disabilities. In this case, ligand biocompatibility testing was more important than chemical toxicity testing. (Table 6) shows the standard values for the haemolytic test.

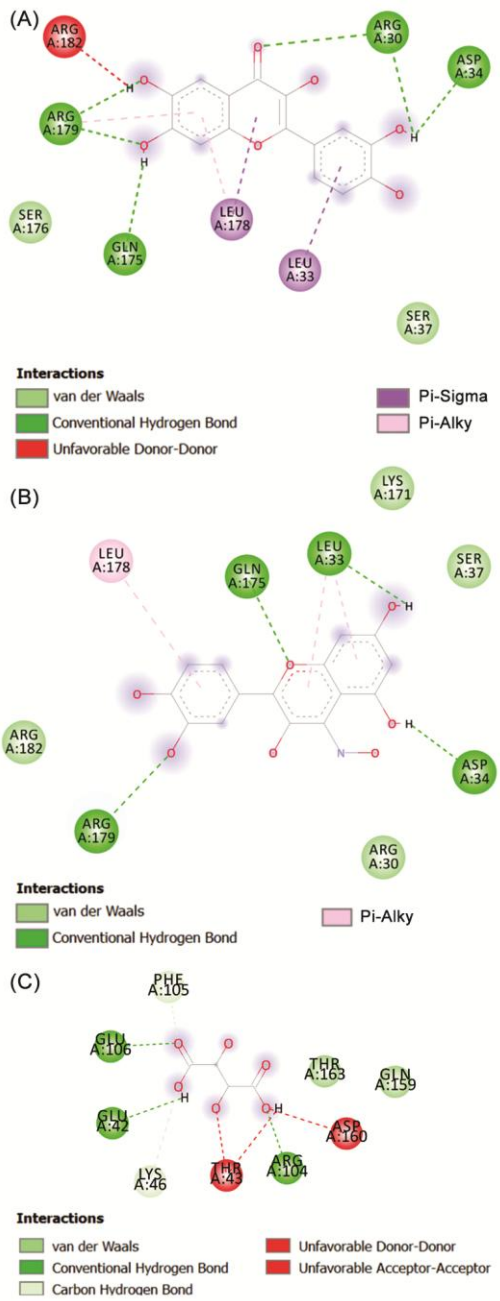

Fig. 4 — (A) 2D interaction of Quercetin IL-6 complex; (B)- 2D interaction of Quercetin oxime IL-6 complex; and (C)- 2D interaction of Tartaric acid IL-6 complex

(Table 7) indicates that all substances were somewhat haemolytic, ranging from 2-10% of the haemolytic index. So, all produced compounds were safer.

Cytotoxicity studies

The MTT assay was performed to screen the metal complexes on Vero cell lines and MCF7 cells, and the results are shown in (Table 8) (Figs 5 & 6). The metal complexes were more cytotoxic toward MCF-7

Table 3 — Synthesized metal complexes

S. No	Compound	Synthesized metal complex
1	QM1	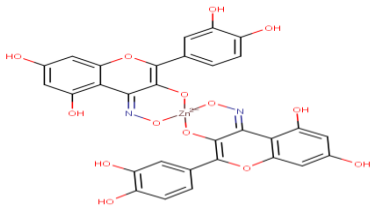
2	QM2	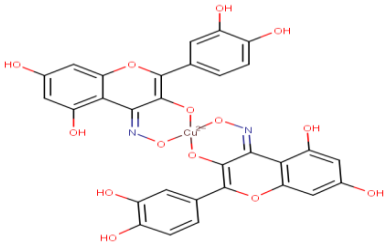
3	QM3	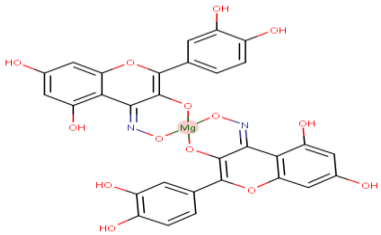
4	QM4	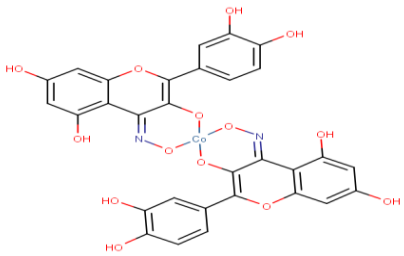
5	QM5	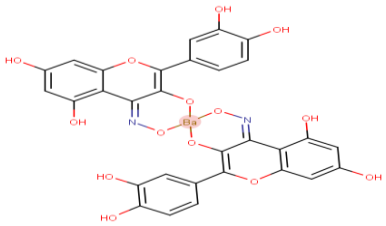
6	QM6	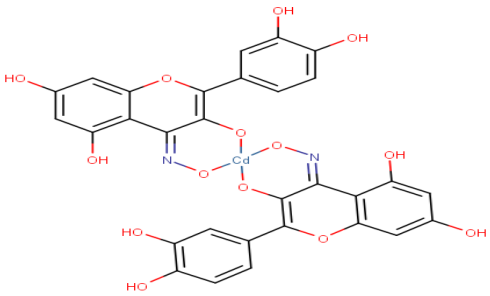

(*Contd.*)

Table 3 — Synthesized metal complexes.(*Contd.*)

S. No	Compound	Synthesized metal complex
7	QM7	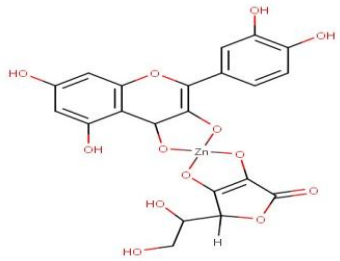

Table 4 — ADME properties of designed compounds

Sample code	Solubility[a]	BBB[b]	CYP2D6[c]	Synthetic accessibility[d]	Absorption[e]	WlogP[f]	TPSA[g]
QM1M1	Moderately soluble	No	No	5.92	Low	3.11	241.94
QM2	Moderately soluble	No	No	5.97	Low	3.11	241.94
QM3	Moderately soluble	No	No	5.4	Low	3.11	241.94
QM4	Moderately soluble	No	No	5.83	Low	3.11	241.94
QM5	Moderately soluble	No	No	5.51	Low	3.11	241.94
QM6	Moderately soluble	No	No	5.91	Low	3.11	241.94
QM7	Soluble	No	No	5.82	Low	0.38	193.83

a) Solubility; b) BBB- Blood-Brain Barrier; c) CYP2D6- Cytochrome 450 inhibition; d) Synthetic accessibility; e) Absorption; f) Wlog P- Partition coefficient of octanal/water system; and g) TPSA- Total Polar surface area.

Table 5 — Toxicity studies for designed compounds

Sample code	Algae test	hERG inhibition	TA100_10RLI	TA1535_10RLI	TA1535_NA	Daphnia
QM1M1	0.000144202	Medium risk	negative	Negative	negative	0.00569073
QM2	0.000237045	Medium risk	negative	Negative	negative	0.0111477
QM4	0.000257791	Medium risk	negative	Negative	negative	0.01631
QM6	0.000237295	Medium risk	negative	Negative	negative	0.0107329
QM7	0.0282117	Medium risk	negative	Negative	negative	0.798832
Limit	<1	---	---	---	---	<1

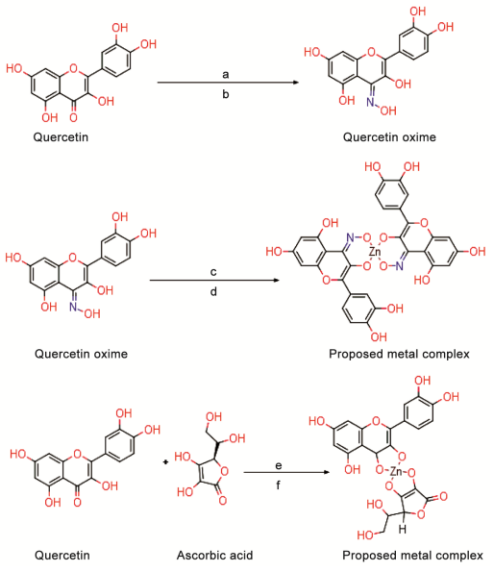

Scheme 1. Synthesis of quercetin oxime from quercetin. Synthesis of proposed metal complexes from quercetin oxime. Synthesis of the proposed metal complex from quercetin and ascorbic acid. Reagents and conditions: (A) Hydroxylamine hydrochloride (NH4OH.HCl), sodium acetate trihydrate (CH3COONa); (B) Ethanol (C2H5OH), reflux 4-5 h; (C) Metal Chlorides [ZnCl2; CuCl2, COCl2, MgCl2, chloride (ZnCl2); and (F) Ethanol, stir for three h

Table 6 —Standard values of Haemolytic assay

Haemolytic index (%)	Haemolytic grade
0-2	Non-haemolytic
2-10	Slightly haemolytic
10-20	Moderately haemolytic
20-40	Markedly haemolytic
>40	haemolytic

Table 7 — Haemolytic assay of synthesized compounds

Compound	Concentration	Absorbance	Haemolytic %
Q	100	2.974	5.217%
	50	2.775	4.713%
	25	1.437	1.326%
QM4	100	2.933	5.113%
	50	2.843	4.886%
	25	1.961	2.653%
QM7	100	3.323	6.101%
	50	3.063	5.443%
	25	2.673	4.455%
QM2	100	3.209	5.812%
	50	2.898	5.025%
	25	2.369	3.754%
DMSO		0.851	0%

Table 8 — Cytotoxicity study of the metal complexes

S. No	Sample code	concentration	% Growth inhibition		CTC_{50} (µg/mL)	
			MCF-7	Vero	MCF-7	Vero
1	QM1	500	74.09	58.79	43.25	159.07
		250	68.32	52.12		
		125	60.89	48.55		
		62.5	56.12	43.26		
		31.25	44.89	38.75		
2	QM7	500	73.80	56.04	48.54	173.01
		250	69.35	53.21		
		125	62.98	48.1		
		62.5	53.98	44.08		
		31.25	42.98	38.00		
3	Std-1 (Nutridac)	500	65.98	56.01	94.78	192.13
		250	60.12	55.75		
		125	54.89	44.99		
		62.5	43.56	40.76		
		31.25	34.32	34.89		

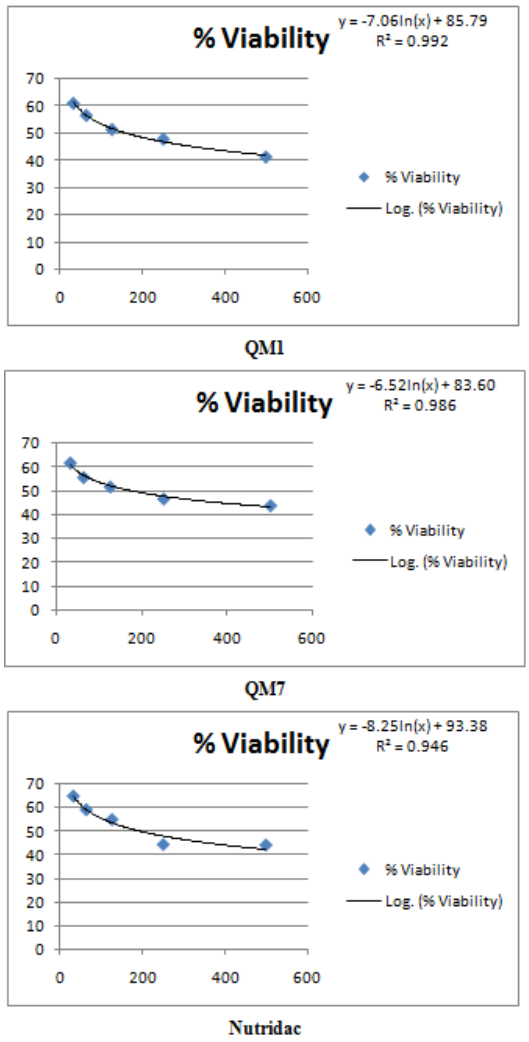

Fig. 5 — Cell viability studies for metal complexes

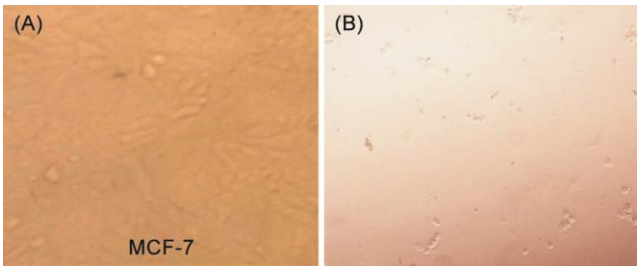

Fig. 6 — (A) MCF-7 cell line without adding drug; and (B) MCF-7 cell line inhibition after addition of drug

cancer cells (IC_{50} values of QM1 and QM7 are 43.25 and 48.54 µg/mL, respectively) and less cytotoxic towards normal Vero cells (IC_{50} value of QM1, QM7 is 159.07, 173.01 µg/mL, respectively). The results obtained were similar to that of the standard (IC_{50} in MCF-7 and Vero cell is 94.78 and 192.13 µg/mL, respectively). The quercetin oxime metal complexes exhibited dose-dependent viability of MCF-7 cells. Quercetin oxime compounds inhibit IL-6 in MCF-7 cells without harming normal cells.The standard drug is Nutridac, which acts as a positive control. All cell culture experiments were performed with cell controls (Negative control) without any treatment. IC_{50} was calculated by comparing the values of cell control.

The percentage growth inhibition was calculated using the formula below:

$$\%\ \text{Growth viability} = \left(\frac{\text{Mean OD of Indiavidual Test Group}}{\text{Mean of OD Control Group}}\right) \times 100$$

Conclusion

It may be inferred that the synthetic metal complexes QM1 and QM7 are superior to Nutridac in inhibiting IL-6. Therefore, flavonoid metal complexes produced in this study have the potential to serve as "LEADs" in the suppression of IL-6 in cytokine storm in COVID-19 patients *via* an inhibitory action on the IL-6 receptor, in addition to performing immunomodulation. In addition to IL-6 directed COVID-19, these complexes may be utilized as "LEADS" to develop new molecules for the treatment of inflammatory auto-immune diseases such as rheumatoid arthritis, juvenile idiopathic arthritis, and giant cell arthritis in the future. However, further molecular research may be carried out to investigate the inhibitory capacity of IL-6.

Acknowledgement

Author Akey Krishna Swaroop expresses his gratitude to JSS College of Pharmacy, JSS Academy of Higher Education and Research.

Conflict of interest

All authors declare no conflict of interest.

References

1 Abbasifard M & Khorramdelazad H, The bio-mission of interleukin-6 in the pathogenesis of COVID-19: A brief look at potential therapeutic tactics. *Life Sci*, 257 (2020) 118097.

2 delRio C & Malani PN, COVID-19-New insights on a rapidly changing epidemic. *JAMA*, 323 (2020) 1339.

3 Tang Y, Liu J, Zhang D, Xu Z, Ji J & Wen C, Cytokine storm in COVID-19: The current evidence and treatment strategies. *Front Immunol*, 11 (2020) 1708.

4 Wu C, Chen X, Cai Y, Xia J, Zhou X, Xu S, Huang H, Zhang L, Zhou X, Du C, Zhang Y, Song J, Wang S, Chao Y, Yang Z, Xu J, Zhou X, Chen D, Xiong W, Xu L, Zhou F, Jiang J, Bai C, Zheng J & Song Y, Risk Factors Associated With Acute Respiratory Distress Syndrome and Death in Patients With Coronavirus Disease 2019 Pneumonia in Wuhan, China. *JAMA Intern Med*, 180 (2020) 934.

5 Yang P, Zhao Y, Li J, Liu C, Zhu L, Zhang J, Yu Y, Wang WJ, Lei G, Yan J & Sun F, Downregulated miR-451a as a feature of the plasma cfRNA landscape reveals regulatory networks of IL-6/IL-6R-associated cytokine storms in COVID-19 patients. *Cell Mol Immunol*, 18 (2021) 1064.

6 Qin C, Zhou L, Hu Z, Zhang S, Yang S, Tao Y, Xie C, Ma K, Shang K, Wang W & Dai-Shi T, Dysregulation of Immune response in patients with Coronavirus 2019 (COVID-19) in Wuhan, China. *Clin Infect Dis*, 71 (2020) 762.

7 Mangalmurti N & Hunter CA, Cytokine storms: understanding COVID-19. *Immunity*, 53 (2020) 19.

8 Ji Y, Ma Z, Peppelenbosch MP & Pan Q, Potential association between COVID-19 mortality and health-care resource availability. *Lancet Glob Health*, 8 (2020) e480.

9 Zhang C, Wu Z, Li JW, Zhao H & Wang GQ, Cytokine release syndrome in severe COVID-19: interleukin-6 receptor antagonist tocilizumab may be the key to reduce mortality. *Int J Antimicrob Agents*, 55 (2020) 105954.

10 Zhou F, Yu T, Du R, Fan G, LiuY, Liu Z, Xiang J, Wang Y, Song B, Gu X, Guan L, Wei Y, Li H, Wu X, Xu J, Tu S, Zhang Y, Chen H & Cao B, Clinical course and risk factors for mortality of adult in patients with COVID-19 in Wuhan, China: a retrospective cohort study. *Lancet*, 395 (2020) 1054.

11 Sinha P, Matthay MA & Calfee CS, Is a "Cytokine Storm" Relevant to COVID-19?. *JAMA Intern Med*, 180 (2020) 1152.

12 Potere N, Batticciotto A, Vecchié A, Porreca E, Cappelli A, Abbate A, Dentali F & Bonaventura A, The role of IL-6 and IL-6 blockade in COVID-19. *Expert Rev Clin Immunol*, 17 (2021) 601.

13 Han H, Ma Q, Li C, Liu R, Zhao L, Wang W, Zhang P, Liu X, Gao G, Liu F, Jiang Y, Cheng X, Zhu C & Xia Y, Profiling serum cytokines in COVID-19 patients reveals IL-6 and IL-10 are disease severity predictors. *Emerg Microbes Infect*, 9 (2020) 1123.

14 Drewett GP, Copaescu A, Mouhtouris E, Hannan N, James F, Smibert O, Holmes NE & Trubiano JA, Evolution of the Human Cytokine Response from Acute Illness to Disease Resolution in SARS-Cov-2 Infection-Implications for Therapeutic Monitoring and Therapeutic Targets. *J Clin Immunol*, 41 (2021) 1162.

15 Angriman F, Ferreyro BL, Burry L, Fan E, Ferguson ND, Husain S, Keshavjee SH, Lupia E, Munshi L, Renzi S & Ubaldo OG, Interleukin-6 receptor blockade in patients with COVID-19: placing clinical trials into context. *Lancet Respir Med*, 9 (2021) 655.

16 Sims NA, Influences of the IL-6 cytokine family on bone structure and function. *Cytokine*, 146 (2021) 155655.

17 Weber R, Groth C, Lasser S, Arkhypov I, Petrova V, Altevogt P, Utikal J & Umansky V, IL-6 as a major regulator of MDSC activity and possible target for cancer immunotherapy. *Cell Immunol*, 359 (2021) 104254.

18 Satarker S, Tom AA, Shaji RA, Alosious A, Luvis M & Nampoothiri M, JAK-STAT pathway inhibition and their implications in COVID-19 therapy. *Postgraduate medicine*, 133 (2021) 489.

19 Solnier J & Fladerer JP, Flavonoids: A complementary approach to conventional therapy of COVID-19?. *Phytochem Rev*, 20 (2021) 773.

20 Oyagbemi AA, Ajibade TO, Aboua YG, Gbadamosi IT, Adedapo AD, Aro AO, Adejumobi OA, Thamahane-Katengua E, Omobowale TO, Falayi OO & Oyagbemi TO, Potential health benefits of zinc supplementation for the management of COVID-19 pandemic. *J Food Biochem*, 45 (2021) e13604.

21 Sabe VT, Ntombela T, Jhamba LA, Maguire GE, Govender T, Naicker T & Kruger HG, Current trends in computer aided drug design and a highlight of drugs discovered *via* computational techniques: A review. *Eur J Med Chem*, 224 (2021) 113705.

22 Stanzione F, Giangreco I & Cole JC, Use of molecular docking computational tools in drug discovery. *Progress Med Chem*, 60 (2021) 273.

23 Baker DHA, An ethnopharmacological review on the therapeutical properties of flavonoids and their mechanisms

of actions: A comprehensive review based on up to date knowledge. *Toxicol Rep*, 9 (2022) 445.

24 daSilva WMB, SDO, Alves DR, deMenezes JESA, Magalhães FEA, Silva FCO, Silva J, Marinho ES & deMorais SM, Synthesis of quercetin-metal complexes, *in vitro* and *in silico* anticholinesterase and antioxidant evaluation, and *in vivo* toxicological and anxiolitic activities. *Neurotox Res*, 37 (2020) 893.

25 Khalid M, Alqarni MH, Foudah AI & Alam P, A high-performance thin-layer chromatography method for the simultaneous determination of quercetin and gallic acid in *Eclipta alba* and *Guiera senegalensis*. *JPC-J Planar Chromat*, 34 (2021) 71.

26 Ali I, Mahmood LM, Mehdar YT, Aboul-Enein HY & Said MA, Synthesis, characterization, simulation, DNA binding and anticancer activities of Co (II), Cu (II), Ni (II) and Zn (II) complexes of a Schiff base containing o-hydroxyl group nitrogen ligand. *Inorg Chem Commun*, 118 (2020) 108004.

27 Selvaraj J, John JBA, Joghee NM, Antony J, Wadhwani A & Natarajan J, Coumarin-fatty acid conjugates as potential ERα/AKT-1 antagonists for er positive breast cancer. *Anticancer Agents Med Chem*, 20 (2020) 437.

28 Denizot F & Lang R, Rapid colorimetric assay for cell growth and survival: modifications to the tetrazolium dye procedure giving improved sensitivity and reliability. *J Immunol Method*s, 89 (1986) 271.

29 Gade R, Priyanka DL, Vijayanandhan V, Shanmugam R, Dharshini SP & Raj K, Polycystic ovarian syndrome (PCOS): Approach to traditional systems, natural and bio-chemical compounds for its management. *Indian J Biochem Biophys*, 59 (2022) 521.

30 Naresh P, Sundar PS, Girija K, Pradheesh SJ, Shanthoshivan AG, Akashwaran S, Swaroop AK & Jubie S, Drug repurposing of Daclatasvir and Famciclovir as antivirals against dengue virus infection by *in silico* and *in vitro* techniques. *Indian J Biochem Biophys*, 58 (2021) 557.